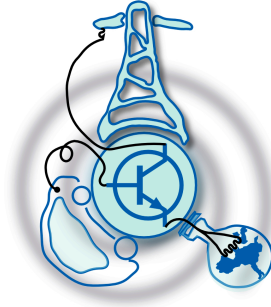# Analysis, Design and Control of Differential Power Processing Converter for Residential PV Integration

by

Miguel Huerta de la Vega

Submitted to the Department of Electrical Engineering, Electronics, Computers and Systems
in partial fulfillment of the requirements for the degree of

Master of Science in Electrical Energy Conversion and Power Systems

at the

UNIVERSIDAD DE OVIEDO

July 2017

Author . . . .

Certified by. . . . .
Pablo García Fernández
Associated Professor
Thesis Supervisor

Analysis, Design and Control of Differential Power Processing Converter for Residential PV Integration

by

Miguel Huerta de la Vega

Submitted to the Department of Electrical Engineering, Electronics, Computers and Systems
on July 20, 2017, in partial fulfillment of the
requirements for the degree of
Master of Science in Electrical Energy Conversion and Power Systems

Abstract

The control of a Differential Power Processing converter for residential photovoltaic installations is addressed in this thesis. With such purpose, the converter was simulated, studied and modelled. Attending at the current state of the art, it was adopted a control strategy suiting the needs of the tricky differential topology, taking advantage of the linear model here developed. The results of the pertinent simulations are evaluated, concluding in high non linearity of the converter topology, and proposing a cascaded control by means of PI controllers that allows the implementation of conventional maximum power point tracking algorithms.

Thesis Supervisor: Pablo García Fernández
Title: Associated Professor

Glossary

Acronyms

DPP	Differential Power Processing
DC	Direct Current
PV	Photovoltaic
MPP	Maximum Power Point
MPPT	Maximum Power Point Tracking
OCC	One-Cycle Control
IC	Incremental Conductance
P&O	Perturb and Observe
PI	Proportional-Integral

Chapter 1

Introduction

Differential Power Processing (DPP) is a DC/DC converter configuration which is placed in parallel with the solar photovoltaic (PV) modules, so it can perform maximum power point tracking (MPPT) while processing only the mismatched power between neighbouring modules. By this means, the overall performance can be improved. Its differential nature favours low power rating in the components of this converter and thus, cheap implementation. Besides, it is possible to implement this topology at submodule-level, being the converters placed in parallel with the strings of a single PV module. [1]

Chapter two offers a review of the state of the art in matter of partial shading, MPPT methods, and the use of DPP converters in PV applications.

Chapter three describes the topology used for the study. Its mathematical model is obtained both in non-linear and linear form. Results of simulations comparing the different models are showed.

Chapter four focuses on the control strategy developed for the DPP converter and the results derived of its implementation.

Finally, chapter five comprises the conclusions observed in this thesis and outlines the future researches to be done.

1.1 Motivations for DPP

In order to obtain the maximum power out of a photovoltaic system, it is required to be able to change the voltage of the PV module so the maximum of the P-V curve is reached (figure 1-1): basically, for a given PV module the amount of current generated depends on the received irradiance and the temperature of the module; the power given by the PV module depends on the voltage in terminals; like figure 1-1 shows, V_{MPP} must be reached. Under normal conditions, there is only one MPP in the PV module, and different techniques are used to track it (figure 1-2).
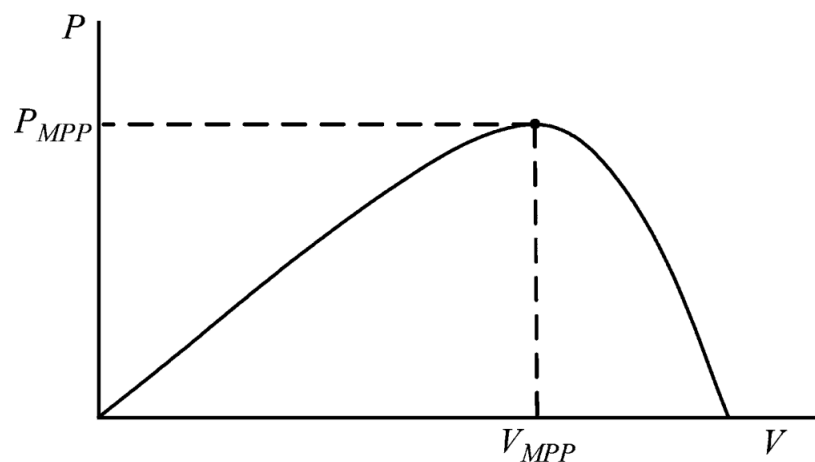

Figure 1-1: Power versus voltage characteristic of a generic PV module. Extracted from [2].

If the MPP wants to be tracked in each PV module, it is needed a DC-DC converter -or a microinverter- per module, so the voltage can be controlled. This can result too expensive in residential applications, where the modules can not perform sun tracking -i.e., they are fixed- and the efficiency improvement is very low. Further, these converters introduce additional power losses. Trying to overcome this issue, a different approach to process the power mismatch was proposed ([3] and [4]), where parallel converters are used. Since the parallel converters bypass the solar modules, they process only the power mismatch between them, being more efficient and cheaper. This technique is called differential power processing.

Under partial shading conditions, very common in residential installations, several

MPPT Technique	PV Array Dependent?	True MPPT?	Analog or Digital?	Periodic Tuning?	Convergence Speed	Implementation Complexity	Sensed Parameters
Hill-climbing/P&O	No	Yes	Both	No	Varies	Low	Voltage, Current
IncCond	No	Yes	Digital	No	Varies	Medium	Voltage, Current
Fractional V_{OC}	Yes	No	Both	Yes	Medium	Low	Voltage
Fractional I_{SC}	Yes	No	Both	Yes	Medium	Medium	Current
Fuzzy Logic Control	Yes	Yes	Digital	Yes	Fast	High	Varies
Neural Network	Yes	Yes	Digital	Yes	Fast	High	Varies
RCC	No	Yes	Analog	No	Fast	Low	Voltage, Current
Current Sweep	Yes	Yes	Digital	Yes	Slow	High	Voltage, Current
DC Link Capacitor Droop Control	No	No	Both	No	Medium	Low	Voltage
Load I or V Maximization	No	No	Analog	No	Fast	Low	Voltage, Current
dP/dV or dP/dI Feedback Control	No	Yes	Digital	No	Fast	Medium	Voltage, Current
Array Reconfiguration	Yes	No	Digital	Yes	Slow	High	Voltage, Current
Linear Current Control	Yes	No	Digital	Yes	Fast	Medium	Irradiance
I_{MPP} & V_{MPP} Computation	Yes	Yes	Digital	Yes	N/A	Medium	Irradiance, Temperature
State-based MPPT	Yes	Yes	Both	Yes	Fast	High	Voltage, Current
OCC MPPT	Yes	No	Both	Yes	Fast	Medium	Current
BFV	Yes	No	Both	Yes	N/A	Low	None
LRCM	Yes	No	Digital	No	N/A	High	Voltage, Current
Slide Control	No	Yes	Digital	No	Fast	Medium	Voltage, Current

Figure 1-2: Summary of the most used MPPT techniques. Extracted from [2].

cells of a PV module receive different level of irradiance than the rest of the module. This situation causes power losses due to the action of the bypass diodes, needed to protect the PV module from hot spots and damage [2]. The bypass diodes can be substituted by small DC optimizers, placed in between the PV module strings, achieving deeper control over the PV module: maximum power point tracking can be performed for each string -i.e., at submodular level-. Submodular DC-DC converters can improve the performance with respect the bypass diodes, but still they have to process al the power of the string, causing some power losses due their efficiency. Thus, DPP is used instead, placed in parallel with each two strings of the PV modules (as it will be seen) to achieve important efficiency improvement at low cost. If a mismatch in the power of the different strings happens, the DPP works by processing the differential power between the adjacent strings so it can be extracted with minimal losses. [1]

9

1.2 Description of DPP

In figure 1-3 it can be seen three different schemes to connect PV modules to the grid; it can be noted that the DPP only needs to process the mismatched power between modules, and even these converters can be turned off if there is no power mismatch at all. This results in increased efficiency of the installation.[1]
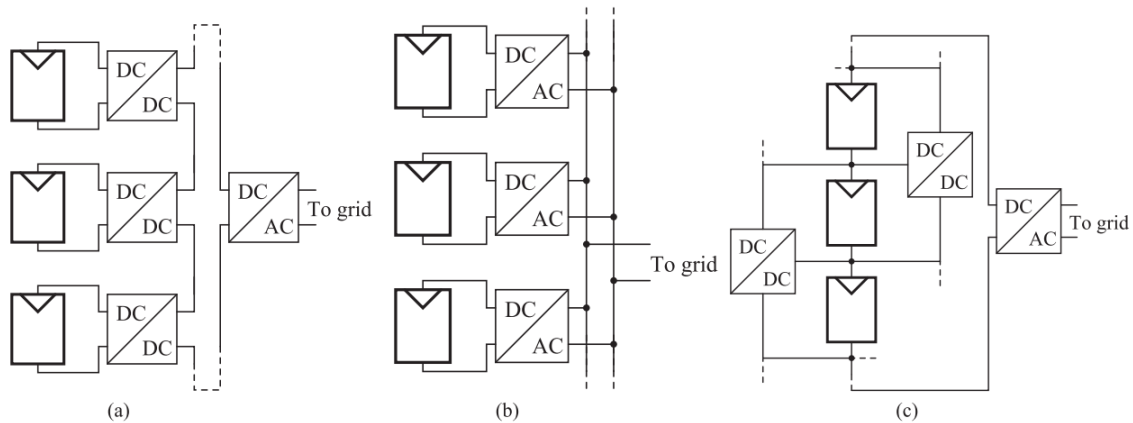

Figure 1-3: Different schemes for MPPT. (a)DC optimizer, (b)microinverter, (c) DPP. Extracted from [1].

Figure 1-4 shows more detailed view of the configuration of the DPP converter: two buck-boost converters are placed in parallel with the PV modules. Also, it could be implemented at submodular level, being the converters placed in parallel with the strings of a single PV module. By means of the DPP converters, it is possible to achieve true MPPT in every module, while the inverter performs MPPT over the whole system; this will ensure extraction of the maximum power.[1]

Regarding the control of the DPP converters, they will be modelled in this thesis so it can be achieved. The study will consider the DPP converters in parallel with PV modules for the sake of simplicity, but the results can be extrapolated to sub-modular DPP applications, where the converters are in parallel with the strings of a PV module; this is important because in a small residential installation, sub-modular DPP approach will make more sense that modular DPP.
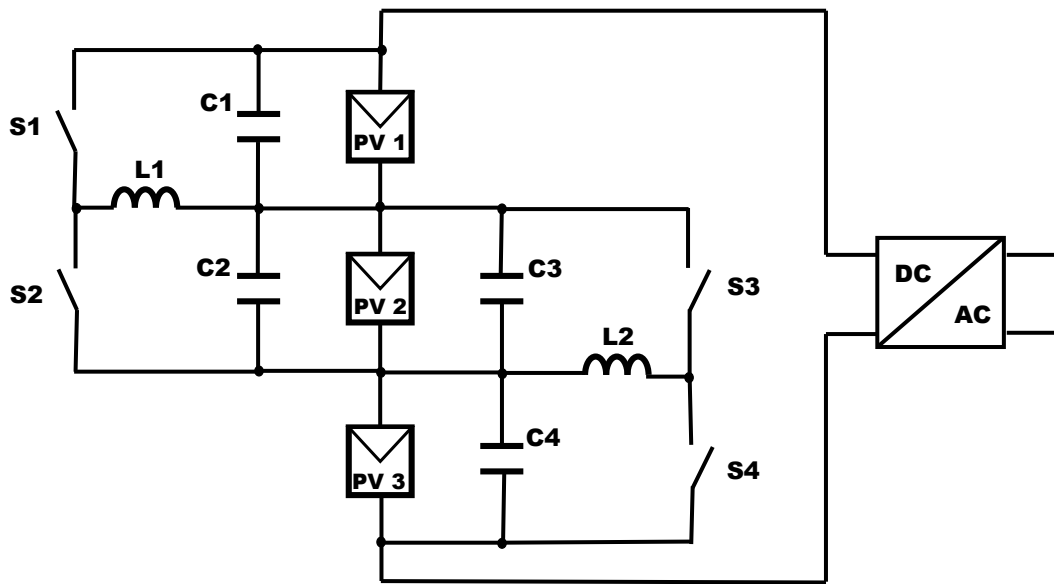
Figure 1-4: DPP converter in detail: buck-boost topology.

Chapter 2

Solutions for partial shading

This chapter offers a deeper explanation of the partial shading effect, how does it affect to the performance of the conventional MPPT methods, and how to overcome it by means of different strategies. The valid MPPT methods to overcome partial shading are explained and compared with the DPP solution.

2.1 Partial shading

Partial shading is quite common situation in residential installations because of trees, buildings and other structures in the surroundings, apart of the common causes like cloudy sky.[1]

Bypass diodes are used to protect the different cell strings in a PV module: when a shade affects some cells in the string of a PV module, the voltage in those cells becomes negative and thus, they start to absorb power; this causes their temperature to increase, creating a hot spot that can damage the PV module. Then, if this situation appears, the bypass diode in the shaded string is turned on, conducting all the current so the shaded cells do not sink any power. In this way the PV module is protected from hot spotting, but the power generated by the non-shaded cells of the string is lost, since the whole string is bypassed by the diode. [5],[6]

The action of the bypass diodes creates different local maximum points in the Power-Voltage curve of the module; this can be appreciated in figure 2-1, where three

PV modules with different irradiances simulate the partial shading in three different strings of a PV module; if partial shading does not exist, there is only one maximum point (fig 2-2). The apparition of these extra maxima can confound the MPP tracking: most of the algorithms used can not detect which of the local maximum are reaching and thus, they can get stuck in one of them without reaching the global maximum -i.e. the MPP-.
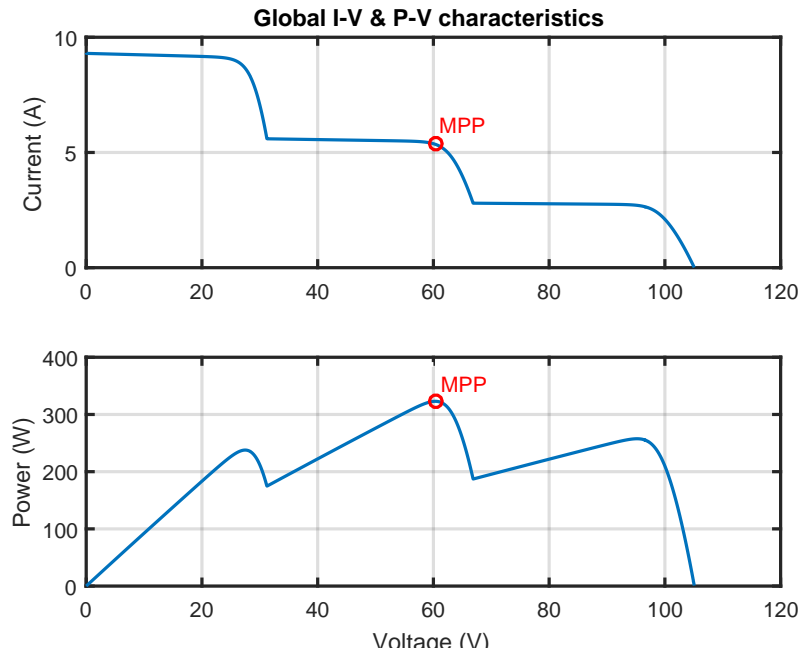

Figure 2-1: Three series PV modules with different irradiances: three local maximum points in P-V curve, one global maximum.

2.2 MPPT methods

In figure 1-2 it was presented a summary of several of the most used MPPT techniques. However, when considering partial shading only a couple of them are adequate. Most of the MPPT strategies are able to find only local maximum, so it is not certain that they will reach the global MPP (fig 2-1). Valid methods for tracking the global MPP under partial shading conditions are: current sweep method, one-cycle control (OCC) MPPT, and two-stage incremental conductance (IC) method.[2]
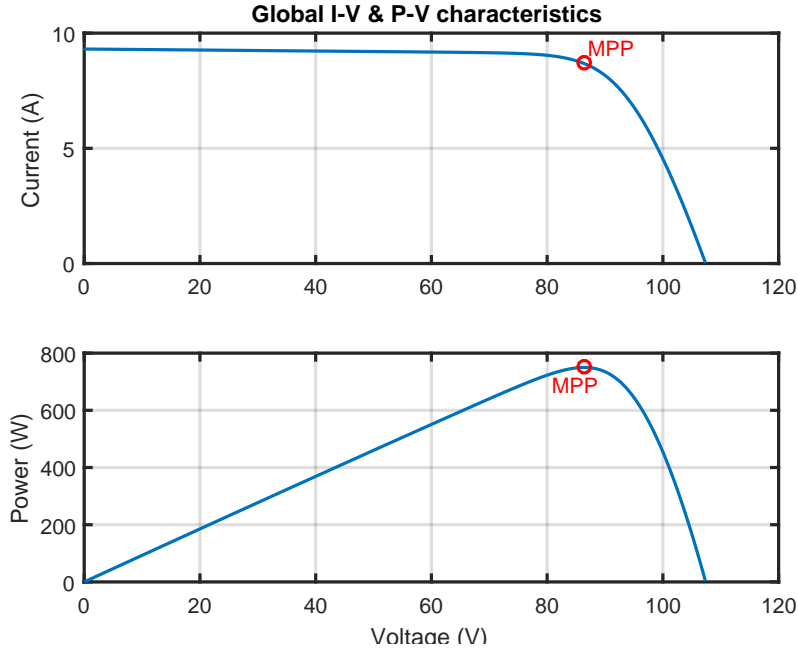
Figure 2-2: Three series PV modules with the same irradiance: only one maximum point.

2.2.1   Two-step incremental conductance method

Incremental conductance method is based on the derivative of the P-V characteristic of a PV module (fig 1-1):

$$\begin{cases} dP/dV > 0 & \text{at the left of MPP} \\ dP/dV = 0 & \text{at the MPP} \\ dP/dV < 0 & \text{at the right of MPP} \end{cases} \tag{2.1}$$

Given that:

$$\frac{dP}{dV} = \frac{d(IV)}{dV} = I + V\frac{dI}{dV} \cong I + V\frac{\Delta I}{\Delta V} \tag{2.2}$$

15

Equation 2.2.1 can be put as:

$$
\begin{cases}
\Delta I/\Delta V > -I/V & \text{at the left of MPP} \\
\Delta I/\Delta V = -I/V & \text{at the MPP} \\
\Delta I/\Delta V < -I/V & \text{at the right of MPP}
\end{cases}
\tag{2.3}
$$

And so, the MPP can be tracked by comparing the instantaneous conductance (I/V) to the incremental conductance $(\Delta I/\Delta V)$ with the algorithm shown in figure 2-3. [2]

The two-step incremental conductance method uses a more complex algorithm that, by monitoring the open-circuit voltage (V_{OC}) and short-circuit current (I_{SC}) of the PV modules, allows to locate the vicinity of the global MPP before executing the standard IC algorithm depicted in figure 2-3; this is achieved by calculating a load resistance close to the optimal one, so the standard IC method can start in the global MPP. ([7],[8]).

2.2.2 Current sweep method

The approach of this method consists in calculating the I-V curve (first plot in figure 2-2) of the PV module each certain intervals of time and obtain from it the voltage corresponding to the MPP (V_{MPP}). It is required $50\,ms$ to carry out the complete operation, in which the operation of the converter is interrupted -i.e., there is no power output-. Because of this inconvenience, it is needed a minimum power threshold to activate the MPP tracker: under this threshold, the power gain that the tracker can achieve is lower than the power lost in the turn-off of the converter. [9]

The sweep waveform is set directly proportional to its derivative:

$$
i(t) = f(t); \qquad f(t) = k\frac{df(t)}{dt}
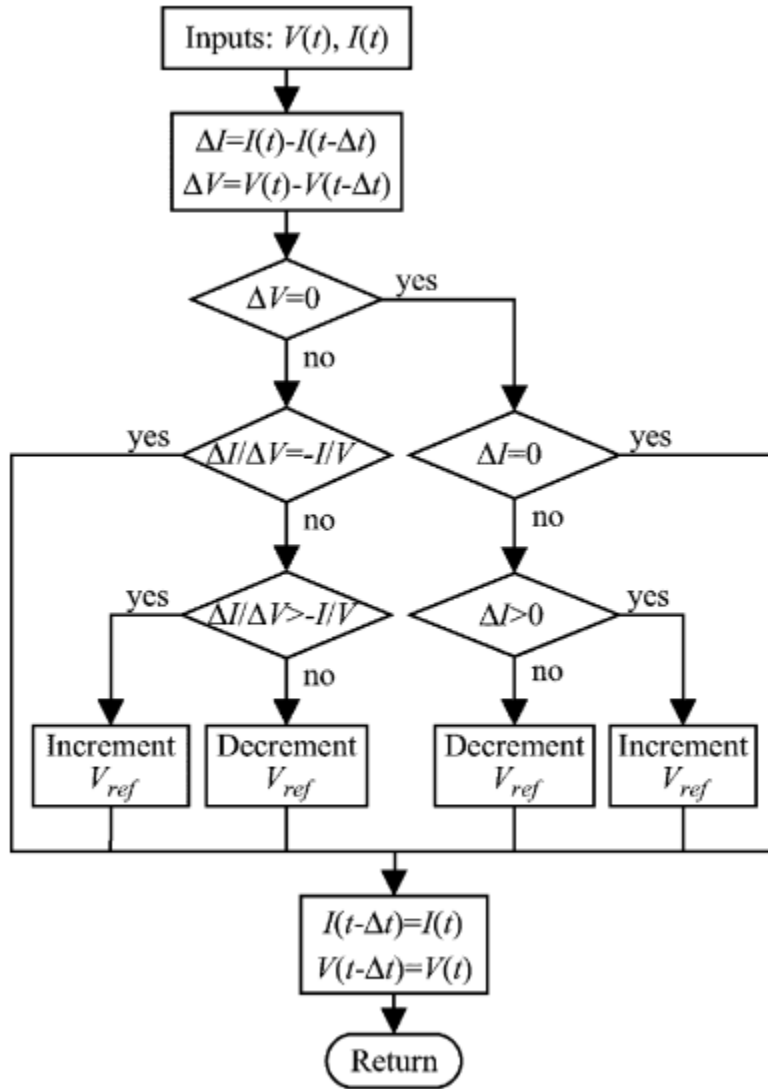\tag{2.4}
$$

Figure 2-3: Algorithm for incremental conductance method. Extracted from [2].

Being the power of the PV module:

$$p(t) = v(t)i(t) = v(t)f(t), \qquad (2.5)$$

at the MPP:

$$\frac{dp(t)}{dt} = v(t)\frac{df(t)}{dt} + f(t)\frac{dv(t)}{dt} = 0 \qquad (2.6)$$

And substituting eq 2.4 in 2.6:

$$\frac{dp(t)}{dt} = \left[v(t) + k \frac{dv(t)}{dt} \right] \frac{df(t)}{dt} = 0 \tag{2.7}$$

The solution of eq 2.4 is unique:

$$f(t) = Ce^{t/k}, \tag{2.8}$$

being C the maximum current of the PV module. Constant (k) is a negative real number. The selection of this both constants can be done by using the discharge current of a capacitor [2],[9].

2.2.3   One-cycle control method

This method is used with a single-stage inverter performing MPPT and regulating the output current, as can be seen in figure 2-4. [10]
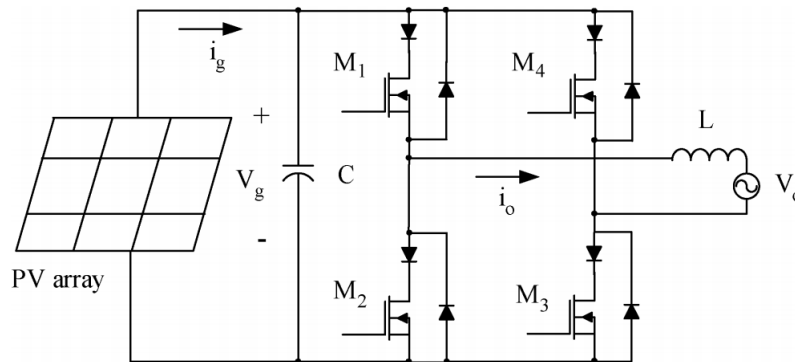
Figure 2-4: Inverter power stage for OCC method. Extracted from [10].

The one-cycle control scheme is showed in figure 2-5. The MPPT is obtained by an arrangement dependent on several constants experimentally determined for each installation ([10]). OCC was designed to obtain instantaneous control of the average value of the switched parameters [11], and in this method it is modified to achieve both MPPT and current output control.
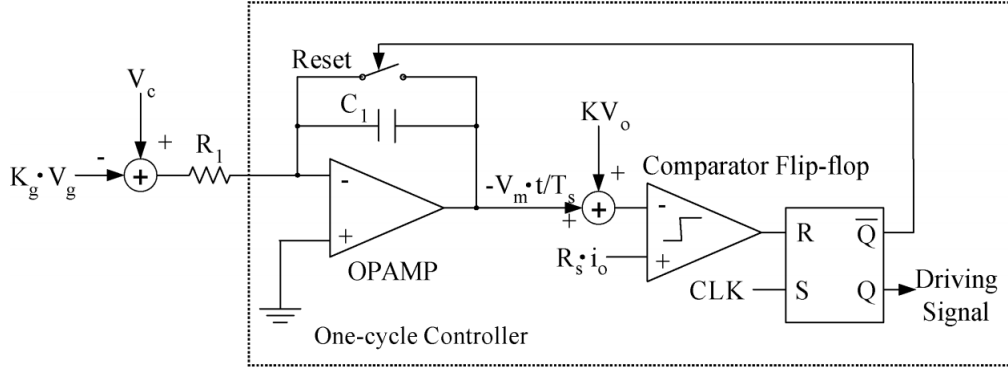
18

Figure 2-5: MPPT implementation with OCC method. Extracted from [10].

2.3   DPP architecture in PV applications

The differential power processing architecture was introduced in solar systems trying to overcome the problems of partial shading between PV modules ([12], [13]), but it was the submodular implementation approach the one with the major advantages, as it will be seen.

The MPPT methods explained in the previous section work in partial shading situations when microinverters or DC optimizers are used individually in each panel (a and b in figure 2-6); but the bypass diodes still generate a power loss that can not be overcome with this approach. That is the reason why DC optimizers at submodular level were developed [14]: they replace bypass diodes between the strings of a PV module so it is possible to perform MPP tracking in each string of the PV module, improving the efficiency up to 20%. They are cheap since they are small enough to be placed in the junction box of the PV module without major efforts.[14]

However, the submodular use of DPP converters instead of DC optimizers can have some advantages ([15], [16]). Because they are differential converters, DPP converters do not process the whole power out of a string, but only the mismatched power between adjacent strings (c in figure 2-6). This feature makes them more desirable than DC optimizers, since they are smaller and cheaper. Besides,as well as submodular DC optimizers, submodular DPPs eliminate the bypass diodes, leaving

hence only one MPP in the P-V curve (fig 2-2), simplifying the MPPT algorithm used. Further than that: the mean time to failure in this topology is higher than others -e.g., DC optimizers and central inverter topologies-, increasing with system size. [15]
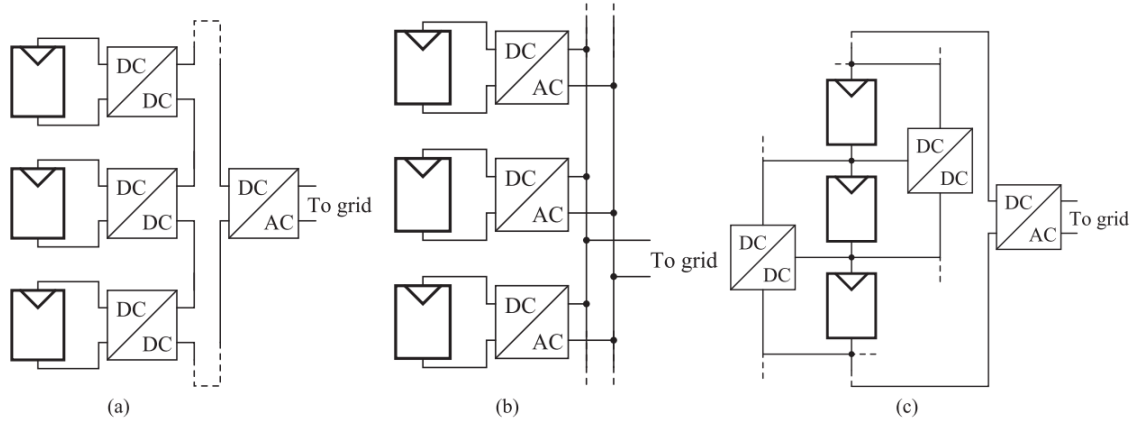

Figure 2-6: Different schemes for MPPT. (a)DC optimizer, (b)microinverter, (c) DPP. Extracted from [1].

Chapter 3

DPP

In order to be able to design a controller for the MPPT of the DPP converter, it is needed first to get a linear model of the converter. The dynamic equations that define the DPP converter are obtained and linearized in this chapter. Additionally, the hardware design is carried out as well as the simulation and comparison between the different models.

3.1   System design

The simulation of the converter requires the power design of the elements used. The characteristics of the PV modules used for the simulation are displayed in table 3.1. For the elements of the converter, it was followed the design proposed in [1]; capacitor and inductor values are all the same; they can be checked in table 3.2. Since the DPP converters only have to process a small part of the total power, it can be used high frequency transistors in order to keep small the size of the magnetic components. This is important because although the simulation was done with DPP converters placed in parallel with PV modules, the advantageous implementation with respect other topologies is in between the strings of the PV modules -i.e.,submodular level-, as discussed in Chapter 2. The results and conclusions of this thesis can be completely extrapolated to submodular level DPP converters.

Table 3.1: PV module parameters

Maximum power	250 W
Open circuit voltage (Voc)	35.8 V
Short-circuit current (Isc)	9.31 A
Voltage at MPP	28.8 V
Current at MPP	8.68 A
Temperature coefficient of Voc	-0.294 %/°C
Temperature coefficient of Isc	0.068 %/°C

Table 3.2: DPP converter design parameters

Capacitor (C)	10 μF
Inductor (L)	10 μH
Switching frequency	300 kHz

3.2 DPP modelling

The dynamic equations of the converter are needed so the linear model can be obtained. In figure 3-1 is showed the buck-boost topology of the DPP converter with all the used currents and voltages indicated.

The currents in the inductors can be written as:

$$I_{L1} = I_{pv1} - I_{pv2} + D_2 I_{L2} - I_{C1} + I_{C2} + I_{C3}$$

$$I_{L2} = I_{pv2} - I_{pv3} + (1 - D_1)I_{L1} - I_{C2} - I_{C3} + I_{C4}$$

$$Since \quad C2 = C3 \quad and \quad V_{C2} = V_{C3} \rightarrow I_{C2} = I_{C3}$$

$$Then:$$

$$I_{L1} = I_{pv1} - I_{pv2} + D_2 I_{L2} - I_{C1} + 2I_{C2} \tag{3.1}$$

$$I_{L2} = I_{pv2} - I_{pv3} + (1 - D_1)I_{L1} - 2I_{C2} + I_{C4} \tag{3.2}$$

The voltages in the capacitors are equal to the one in the PV modules, so:

$$V_{pv2} = \frac{1}{C} \int I_{C2}\, dt; \qquad V_{pv3} = \frac{1}{C} \int I_{C4}\, dt \tag{3.3}$$
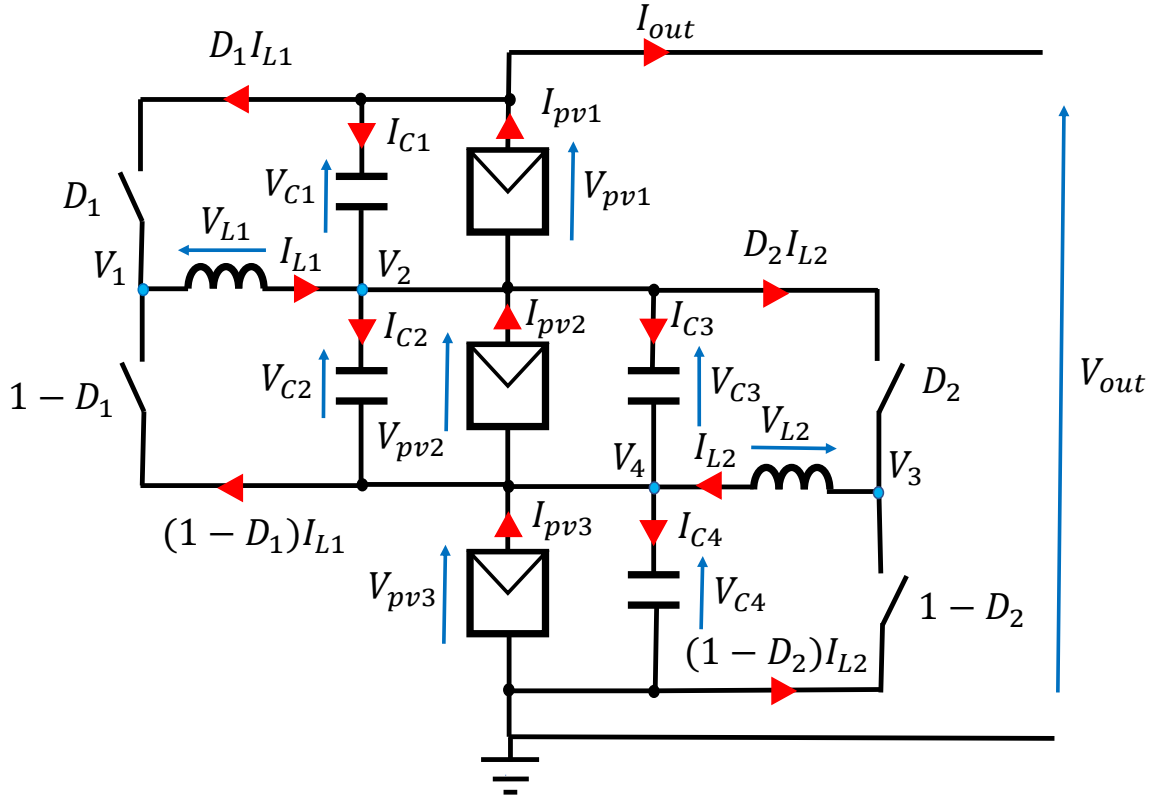
Figure 3-1: Currents and voltages in DPP converter. Note that $V_{L1} = V_1 - V_2$ and $V_{L2} = V_3 - V_4$.

As said, since all the capacitors has the same value (table 3.2), the currents in the capacitors 2 and 3 are equal ($I_{C2} = I_{C3}$ in fig 3-1). Since capacitor 2 ($C2$) belongs to the first converter -DPP1- and capacitor 3 ($C3$) belongs to the second one -DPP2- and both two have the same voltage, it exists a coupling between the two converters. This is going to complicate the linear modelling and therefore the current and voltage control.

It can be noted that in equation 3.3 the voltage in the first PV module, V_{pv1} was omitted. This is because it is already defined with the voltage set by the inverter (V_{out}); the inverter is going to have its own MPPT for the string of PV modules. So,

$$V_{pv1} = V_{out} - V_{pv2} - V_{pv3} \tag{3.4}$$

In this way, with the addition of the voltage set by the microinverter (V_{out}) it is possible to define a voltage control for two of the PV modules by controlling the currents in the two inductors; otherwise, it would be impossible, since in this kind of topology, the PV modules are always going to outnumber the converters by one.

Finally, it can be obtained from the circuit (fig 3-1) the following relations that are going to be useful later on:

$$I_{out} = I_{pv1} - D_1 I_{L1} - I_{C1} \tag{3.5}$$

$$V_1 = D_1 V_{out} + (1 - D_1) V_{pv3}; \qquad V_2 = V_{pv2} + V_{pv3} \tag{3.6}$$

$$V_3 = D_2 (V_{pv2} + V_{pv3}); \qquad V_4 = V_{pv3} \tag{3.7}$$

3.3 Simulation

The simulation of the circuit was carried out in MatLab® Simulink®. In figure 3-2 it can be seen the circuit modelled in the Simulink environment; the solar modules are from MatLab library (included since version R2015a) and are modelled like figure 3-3 shows.

A non-linear model was developed and implemented as a block diagram so it can be linearized (figure 3-4). The model was verified with the circuit simulation. The inputs are marked in blue, which are: duty cycles of the two converters (D_1, D_2), the currents in the PV modules (I_{pv1}, I_{pv2}, I_{pv3}), and the output current and voltage (I_{out}, V_{out}). As said, voltage in the first PV module is function of the other three: $V_{pv1} = V_{out} - V_{pv2} - V_{pv3}$, so it does not appear on the diagram. Also, realize that $V_{L1} = V_1 - V_2$ and $V_{L2} = V_3 - V_4$, as depicted in figure 3-1.

The non-linear model was constructed from the previous equations (3.1, 3.2, 3.3, 3.4, 3.5, 3.6, 3.7), arranging them in the following way (fig 3-4):
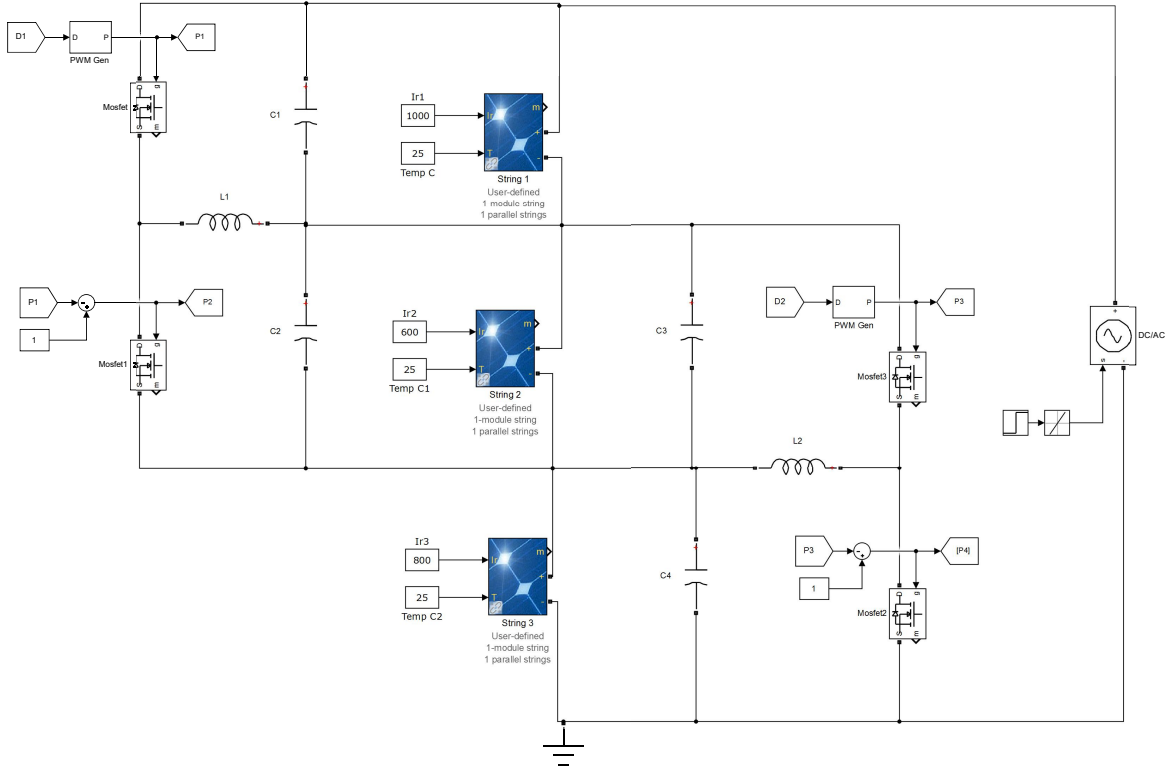
24

Figure 3-2: DPP converters circuit in Simulink. The inverter is modelled as a constant voltage source.

$$V_{L1} = V_1 - V_2 \quad \rightarrow \quad I_{L1} = \frac{1}{L} \int V_{L1} dt$$

$$I_{C2} = \frac{1}{2}(I_{pv2} - I_{pv1} + \underline{I_{C1}} + I_{L1} - D_2 I_{L2})$$

$$I_{C1} = I_{pv1} - I_{out} - D_1 I_{L1}$$

$$V_{pv2} = \frac{1}{C} \int I_{C2} dt \quad \rightarrow \quad V_2 = V_{pv2} + V_{pv3} \quad \rightarrow \quad V_3 = D_2 V_2$$

$$V_{L2} = V_3 - V_4 \quad \rightarrow \quad I_{L2} = \frac{1}{L} \int V_{L2} dt$$

$$I_{C4} = I_{pv3} - I_{pv2} + 2I_{C2} + I_{L2} - (1 - D_1)I_{L1}$$

$$V_{pv3} = \frac{1}{C} \int I_{C4} dt \quad \rightarrow \quad V_4 = V_{pv3} \quad \rightarrow \quad V_1 = D_1 V_{out} + (1 - D_1)V_{pv3}$$
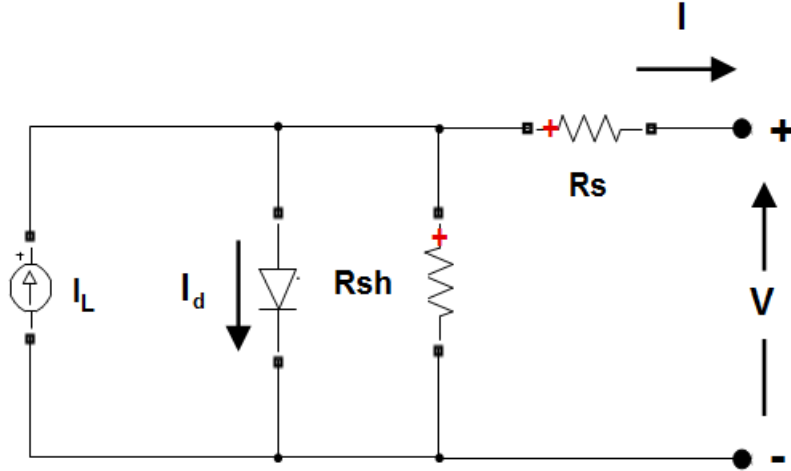
Figure 3-3: PV array block in Simulink; five parameter model using: light-generated current, diode saturation current and ideality factor, shunt resistance, and series resistance.[17]

Notice that equation 3.5 was introduced so the measurement of I_{C1} could be avoided. The only measurements in the model (fig 3-4) are the currents in the PV modules (I_{pv1}, I_{pv2}, I_{pv3}), the output current (I_{out}), and the output voltage (V_{out}). The parameter $R_L = 0.05\,\Omega$ is not part of the circuit; it was introduced in the model so it became stable. However, the introduction of this parameter does not affect the accuracy of the results.

3.3.1 Linearization

With the non-linear model validated, the linear model was obtained by means of the state space model. The state space model was obtained from the equations, and then it was verified with the state space model provided by Linear Analysis tool in Simulink. With the state space model in MatLab is straightforward to obtain the transfer functions between any input and output.

The states in the non-linear model (figure 3-4) are: $I_{L1}, V_{pv2}, I_{L2}, V_{pv3}$. And the
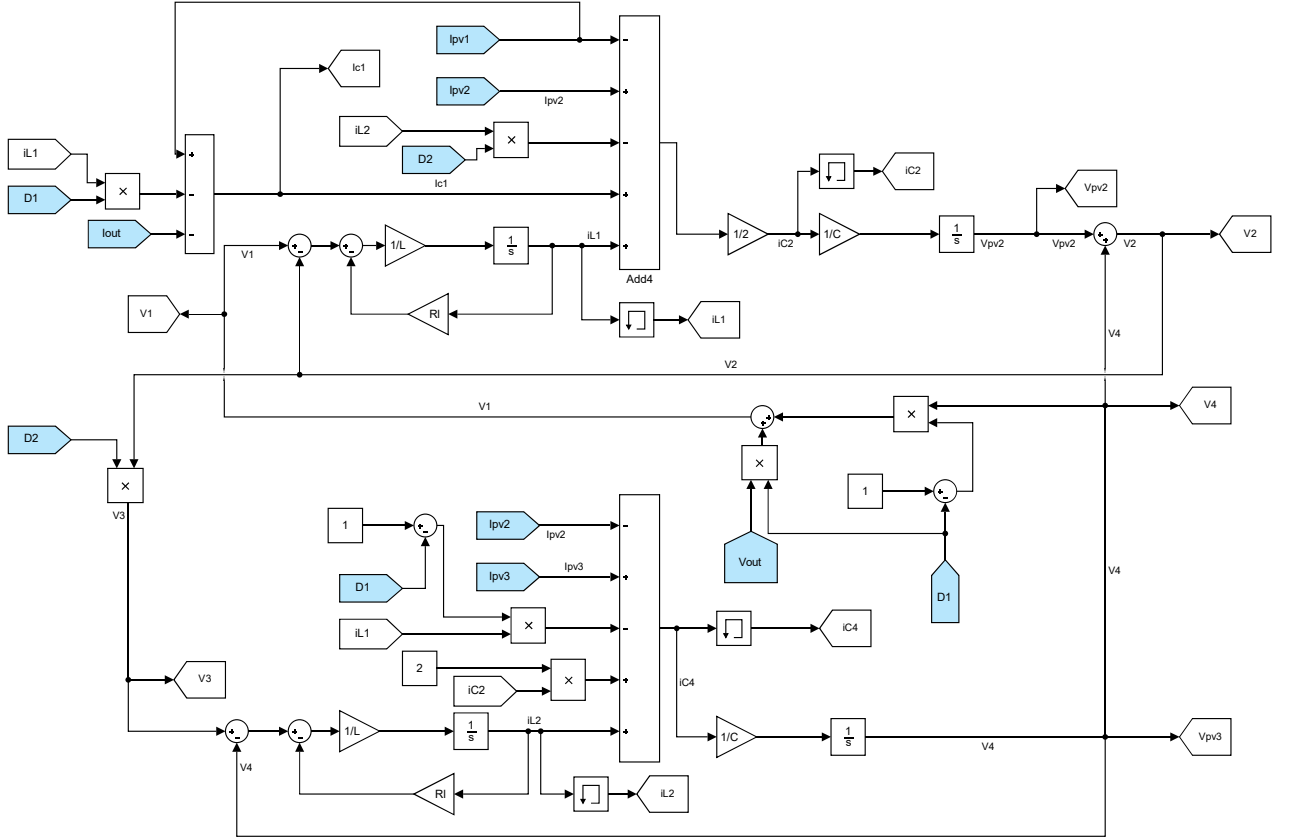
Figure 3-4: DPP non-linear model. External inputs in blue. Memory blocks added in feedback loops.

non-linear equations obtained:

$$\dot{I}_{L1} = \frac{1}{L}\big(-R_L I_{L1} + D_1(V_{out} - V_{pv3}) - V_{pv2}\big) \tag{3.8}$$

$$\dot{V}_{pv2} = \frac{1}{2C}\big(I_{pv2} - I_{out} + (1 - D_1)I_{L1} - D_2 I_{L2}\big) \tag{3.9}$$

$$\dot{I}_{L2} = \frac{1}{L}\big(-R_L I_{L2} + D_2 V_{pv2} + (D_2 - 1)V_{pv3}\big) \tag{3.10}$$

$$\dot{V}_{pv3} = \frac{1}{C}\big(I_{pv3} - I_{out} + (1 - D_2)I_{L2}\big) \tag{3.11}$$

Notice that in the fourth state from figure 3-4, $I_{C2} = \frac{1}{2}\big(I_{pv2} - I_{out} + (1 - D_1)I_{L1} - D_2 I_{L2}\big)$; thus, equation 3.11 was obtained.

27

Now, linearizing this equations (3.8, 3.9, 3.10 and 3.9) it is obtained:

$$\Delta \dot{I}_{L1} = \frac{1}{L}\left(-R_L\Delta I_{L1} + \Delta D_1(V_{out}^o - V_{pv3}^o) - \Delta V_{pv2} + D_1^o\Delta V_{out} - D_1^o\Delta V_{pv3}\right) \quad (3.12)$$

$$\Delta \dot{V}_{pv2} = \frac{1}{2C}\left(\Delta I_{pv2} - \Delta I_{out} + (1 - D_1^o)\Delta I_{L1} - D_2^o\Delta I_{L2} - I_{L1}^o\Delta D_1 - I_{L2}^o\Delta D_2\right)$$
$$(3.13)$$

$$\Delta \dot{I}_{L2} = \frac{1}{L}\left(-R_L\Delta I_{L2} + \Delta D_2(V_{pv2}^o + V_{pv3}^o) + (D_2^o - 1)\Delta V_{pv3}\right) \quad (3.14)$$

$$\Delta \dot{V}_{pv3} = \frac{1}{C}\left(\Delta I_{pv3} - \Delta I_{out} + (1 - D_2^o)\Delta I_{L2} - I_{L2}^o\Delta D_2\right) \quad (3.15)$$

The superscript $(^o)$ in the linearized equations (3.12, 3.13, 3.14, 3.15) indicates the variables evaluated in the equilibrium point. Then, the state space model can be obtained, and it is valid for the neighbouring of the equilibrium point, whichever is selected. From the state space model, it is easy with the help of MatLab to obtain the transfer functions between the inputs and the different outputs that are going to be dependent on the selected equilibrium point. So, the linear model, implemented by means of the state space, should have the same behaviour that the non-linear model near the equilibrium point.

Following:

$$\begin{cases} \dot{x} = Ax + Bu \\ y = Cx + Du \end{cases}$$

$$x = \begin{bmatrix} I_{L1} \\ V_{pv2} \\ I_{L2} \\ V_{pv3} \end{bmatrix} \qquad u = \begin{bmatrix} D_1 \\ D_2 \end{bmatrix} \qquad y = x$$

where x is the state matrix, u is the input matrix, and y is the output matrix, which is equal to the state matrix, the matrices A, B, C and D are defined in equation 3.16.

$$A = \begin{bmatrix} \frac{-R_L}{L} & \frac{-1}{L} & 0 & \frac{-D_1^o}{L} \\ \frac{1-D_1^o}{2C} & 0 & \frac{-D_2^o}{2C} & 0 \\ 0 & \frac{D_2^o}{L} & \frac{-R_L}{L} & \frac{D_2^o-1}{L} \\ 0 & 0 & \frac{1-D_2^o}{C} & 0 \end{bmatrix} \qquad B = \begin{bmatrix} \frac{V_{out}^o-V_{pv3}^o}{L} & 0 \\ \frac{-I_{L1}^o}{2C} & \frac{-I_{L2}^o}{2C} \\ 0 & \frac{V_{pv2}^o+V_{pv3}^o}{L} \\ 0 & \frac{-I_{L2}^o}{C} \end{bmatrix}$$

$$C = \begin{bmatrix} 1 & 0 & 0 & 0 \\ 0 & 1 & 0 & 0 \\ 0 & 0 & 1 & 0 \\ 0 & 0 & 0 & 1 \end{bmatrix} \qquad D = \begin{bmatrix} 0 & 0 \\ 0 & 0 \\ 0 & 0 \\ 0 & 0 \end{bmatrix} \tag{3.16}$$

A simulation was done in Simulink with regard to compare the response of the circuit, the non-linear model and the linear model. The comparison between the response of the models developed is showed in figure 3-5; specifically, it is the response of the voltage in PV module number 2 to perturbations in duty cycles. In the image it can be seen the small increment ($\Delta D = 0.1$) in the duty values and the response of the three systems. It can be appreciated almost no difference between the circuit and the non-linear response, reacting equally to the duty increments, but a great dissonance between the former two and the linear model.

All the four states of the model have that bad behaviour, as can be checked in figures 3-7 and 3-8, where the four states of the models are showed when the duty is incremented like in figure 3-5. Further, the inaccuracy is persistent even with smaller ($\Delta D = 0.01$) variations of the duty cycle. This can be seen in figure 3-6, where by zooming in it can be noted a similar behaviour to that in figure 3-5.

3.4   Results

The results of the simulation showed above prove the great non-linear nature of the DPP converter. It is impossible to obtain a decent approximation of the system by using the linear model, since it seems to be inaccurate even with the smallest duty
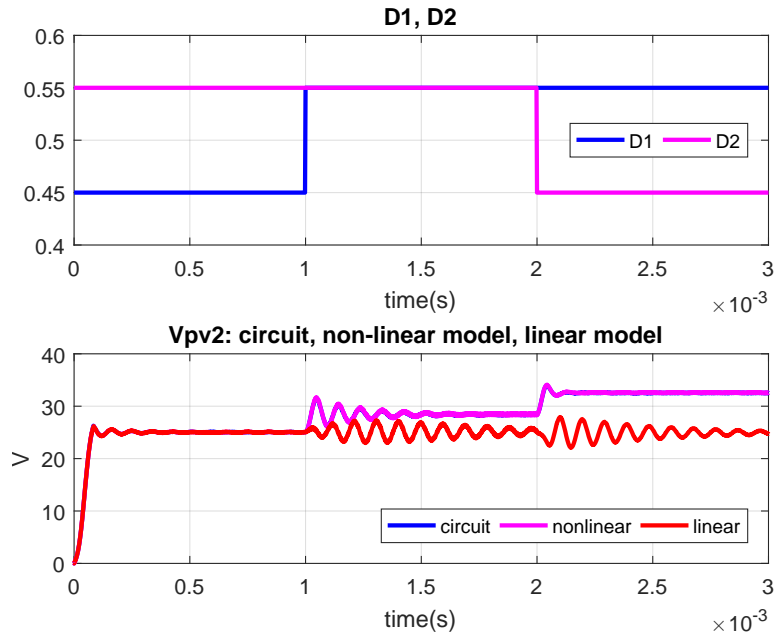
Figure 3-5: Duty cycle perturbation in both converters and voltage in PV module number 2 for the three models in Simulink.
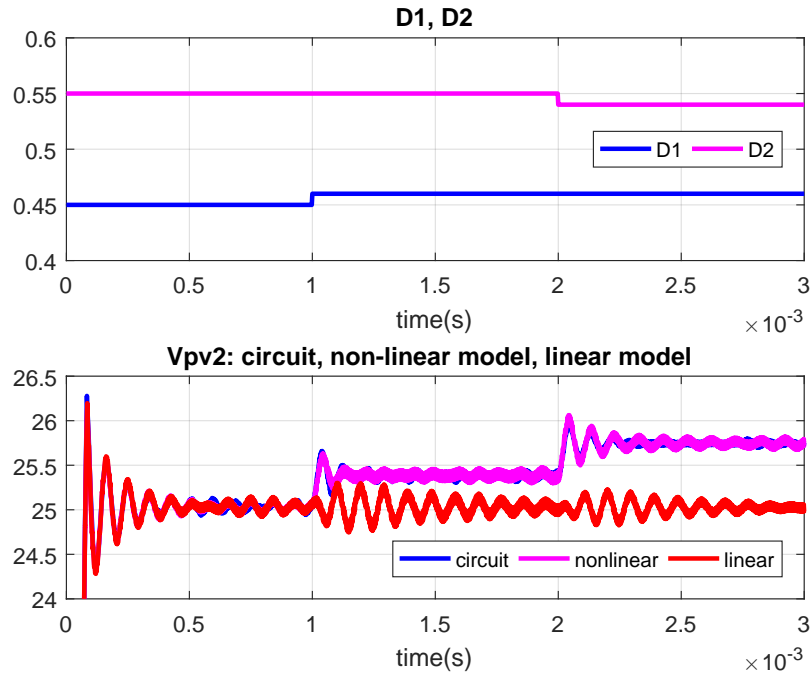

Figure 3-6: Smaller duty cycle perturbation in both converters and voltage in PV module number 2 for the three models in Simulink.
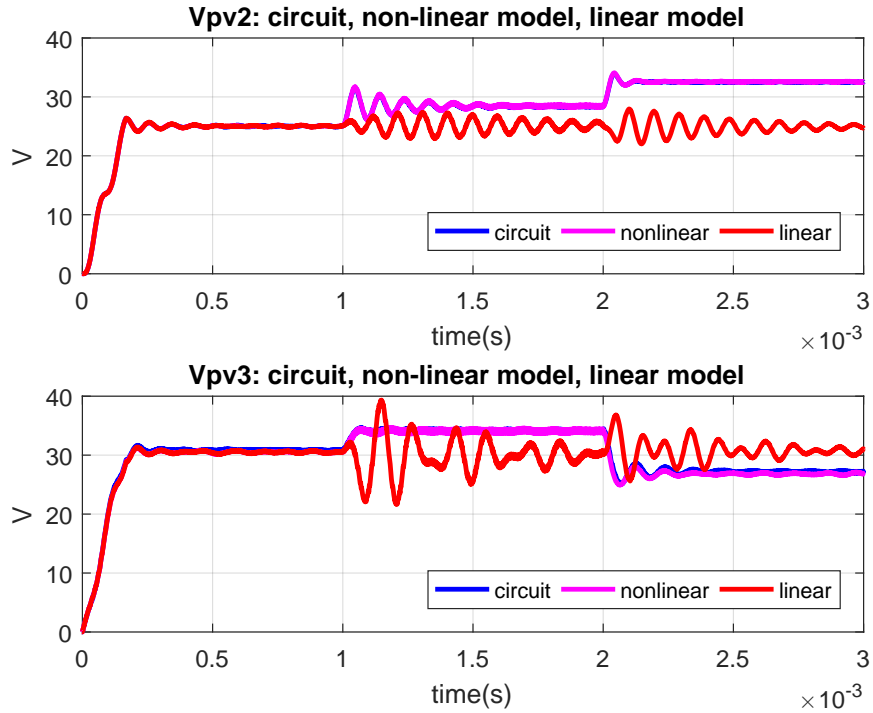
Figure 3-7: Voltages in modules 2 and 3 with 0.1 duty perturbation.

changes.

However, if the duty values in the equilibrium point (D_1^o, D_2^o) can be updated, the model becomes accurate. Of course, if this is done the model is not linear anymore, but it is worth to mention that those values are the only ones making the model inaccurate.

To prove this, it was done a simulation implementing the linear equations ((3.12, 3.13, 3.14, 3.15)) in Simulink (figure 3-9), but modifying the the duty values in the equilibrium point (D_1^o, D_2^o) so they can be updated (figure 3-10). In this way, the response obtained is really good, as can be noticed by the simulation depicted in figure 3-11.
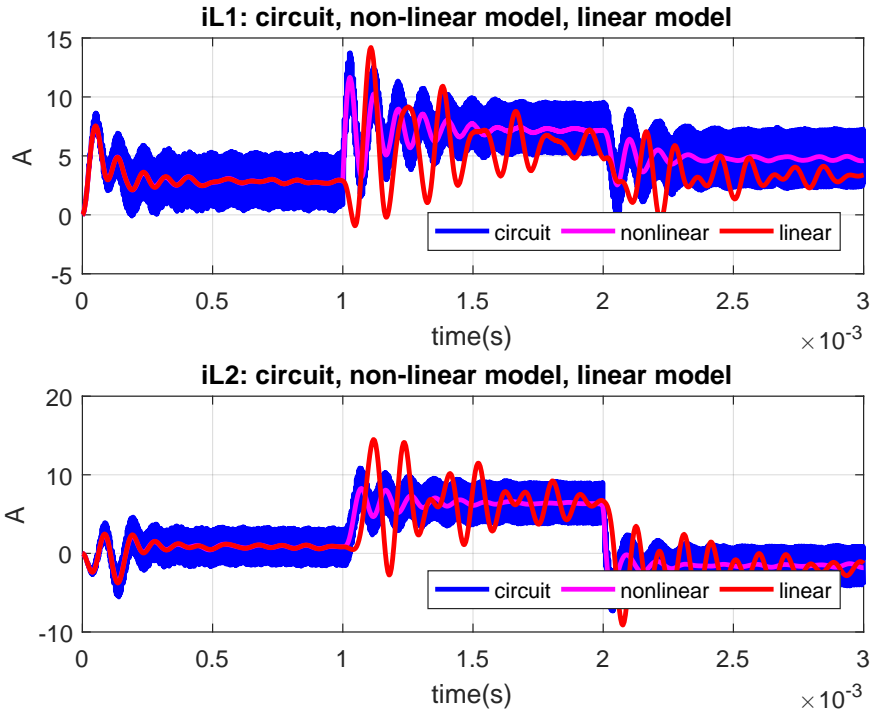
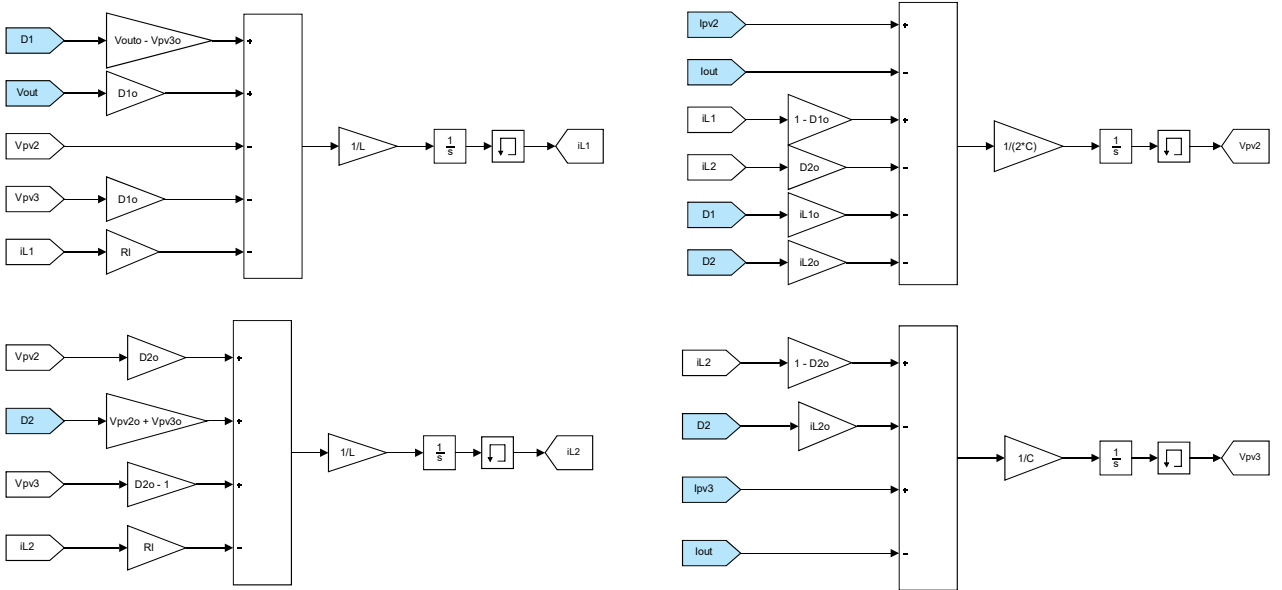Figure 3-8: Currents in the two inductors with 0.1 duty perturbation.

Figure 3-9: Linear model equations in Simulink. Inputs marked in blue. Delays implemented in feedback paths.
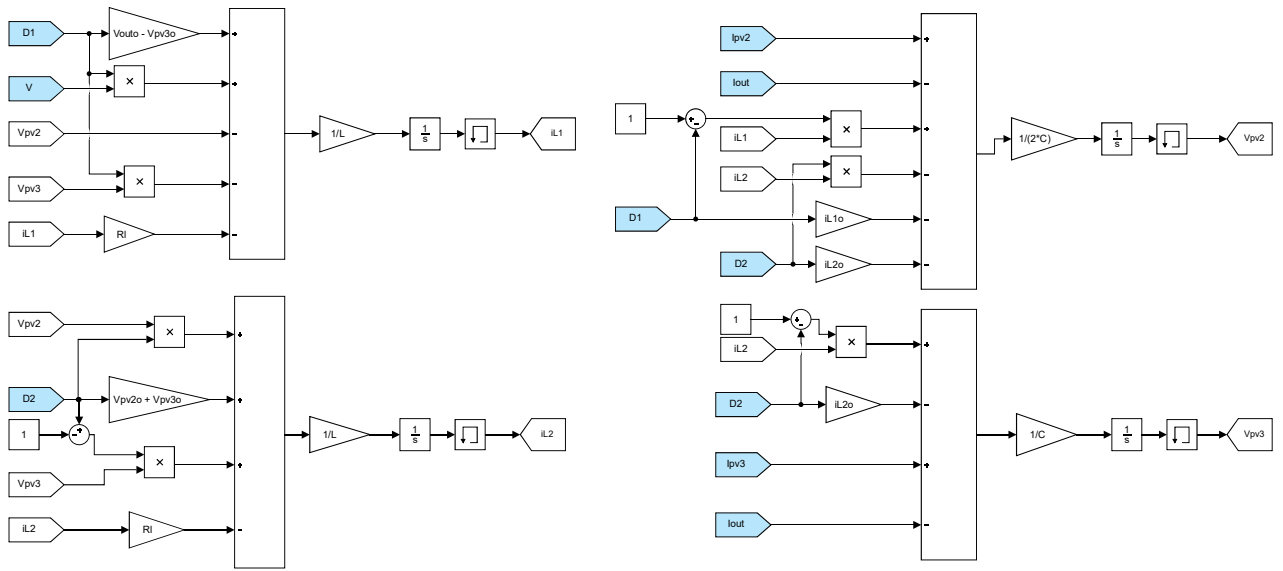
Figure 3-10: Linear model equations with duty cycle equilibrium values updated in Simulink. Inputs marked in blue. Delays implemented in feedback paths.
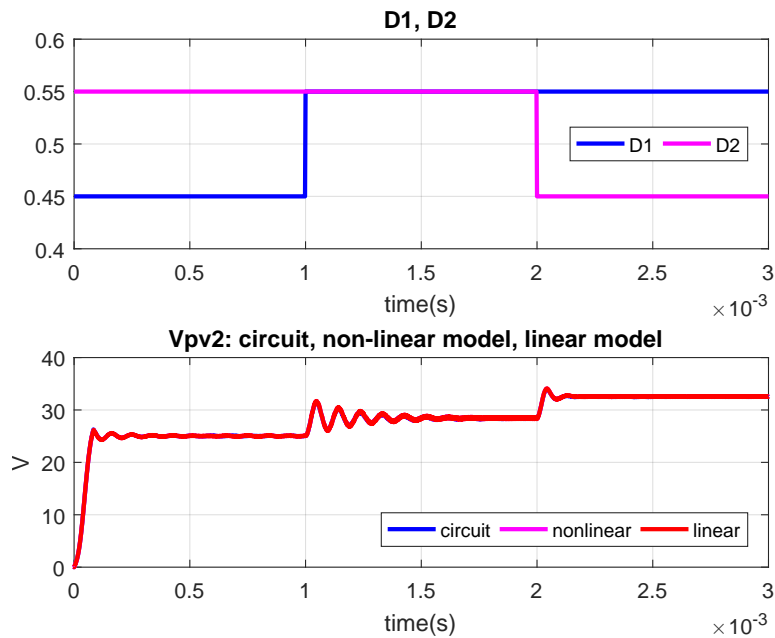

Figure 3-11: Duty cycle perturbation in both converters and voltage in PV module number 2 for the three models in Simulink (modified linear model as in fig 3-10).

Chapter 4

Control System Design

In this chapter it is addressed the main issue of the thesis, which is the control of the DPP converter. The control methods proposed in literature are quite complicated, so a cascaded control by means of PI regulators is explained. The results of the simulation show the validity of the proposed approach.

4.1 Control methods

The DPP converter can be run with fixed duty of $D_1 = D_2 = 0.5$ to attain voltage equalization, which can be a suitable solution if the mismatch in irradiance between strings is not very high. Since DPP converters would be substituting bypass diodes, the power loss would be very low, with an important increment in efficiency ([1]).

However, it has been said that the irradiance mismatch due to partial shading is quite prominent in residential applications, so the control architecture needed gets more complicated. In [18], the proposed algorithm is based in implementing a classic perturb and observe (P&O) algorithm in each DPP converter, trying to maximize the output voltage (V_{out}) for a given output current (I_{out}), which is given by the irradiance received by the strings. The coupling between the converters is solved by means of neighbouring communication, so a given DPP has information about how a duty perturbation in the near converters affects to their voltage. For achieving such a cooperated performance, it is needed a fairly complex algorithm.

The proposed control in this thesis is a cascaded controller with an inner current control loop and an outer voltage control loop. The voltage commands can be given by classic MPPT algorithms.

4.2 Control design

With the linearized equations of the DPP converter it is possible to implement a cascaded control loop using PI controllers. The controlled variables are the currents in the inductors (i_{L1}, i_{L2}) and the voltages in PV modules 2 and 3 (V_{pv2}, V_{pv3}); this is, the states of the linear model. As said, the voltage in the PV module 1 is going to be determined with the global MPPT voltage: $V_{pv1} = V_{out} - V_{pv2} - V_{pv3}$. In figure 4-1 it is showed the described control scheme.
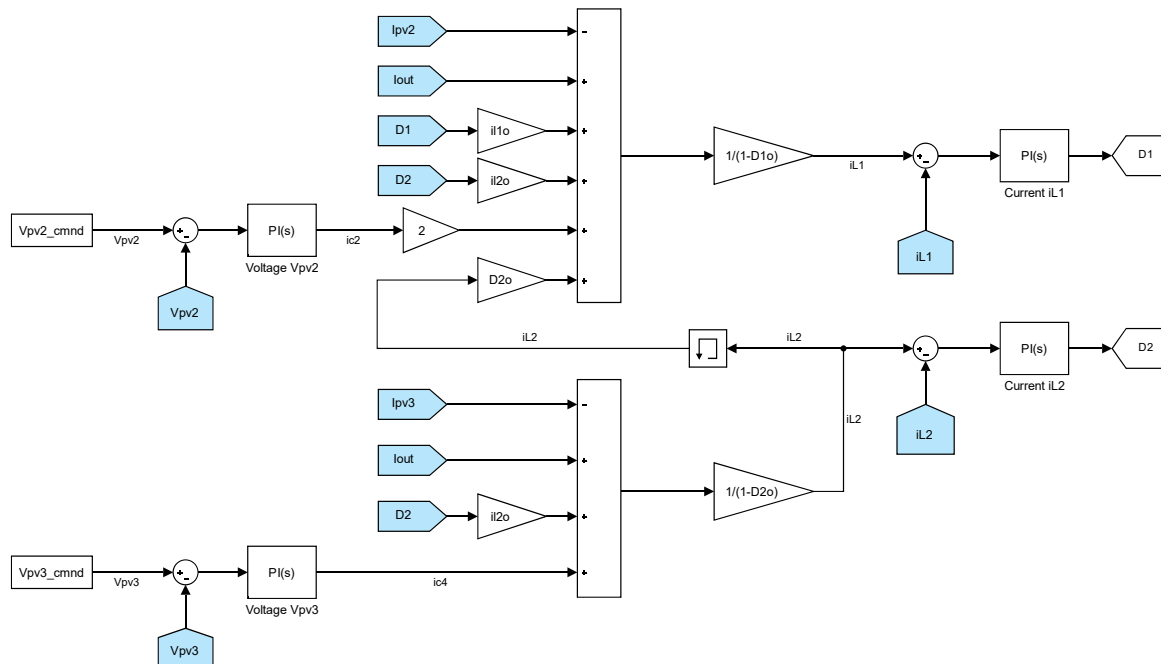

Figure 4-1: Cascaded control scheme of the DPP converter.

4.2.1 Current control

Using equations 3.12 and 3.14 it is possible to obtain the duty cycle from the current in the inductor:

$$\begin{cases} \Delta \dot{I}_{L1} = \frac{1}{L}\left(-R_L\Delta I_{L1} + \Delta D_1(V_{out}^o - V_{pv3}^o) - \Delta V_{pv2} + D_1^o\Delta V_{out} - D_1^o\Delta V_{pv3}\right) \\ \Delta \dot{I}_{L2} = \frac{1}{L}\left(-R_L\Delta I_{L2} + \Delta D_2(V_{pv2}^o + V_{pv3}^o) + (D_2^o - 1)\Delta V_{pv3}\right) \end{cases}$$

Due to the faster dynamics in the current compared to the voltage, it is possible to simplify the former equations:

$$\begin{cases} \Delta \dot{I}_{L1} = \frac{1}{L}\left(-R_L\Delta I_{L1} + \Delta D_1(V_{out}^o - V_{pv3}^o)\right) \\ \Delta \dot{I}_{L2} = \frac{1}{L}\left(-R_L\Delta I_{L2} + \Delta D_2(V_{pv2}^o + V_{pv3}^o)\right) \end{cases} \tag{4.1}$$

Thus, from the previous equations (4.1), the Laplace transform of the duty in function of the inductor current can be obtained:

$$\frac{I_{L1}}{D_1} = \frac{\frac{V_{out}^o - V_{pv3}^o}{L}}{\frac{R_L}{L} + s}; \qquad \frac{I_{L2}}{D_2} = \frac{\frac{V_{pv2}^o + V_{pv3}^o}{L}}{\frac{R_L}{L} + s} \tag{4.2}$$

Now the PI controller can be tuned simply by applying zero pole cancellation over the obtained plants.

4.2.2 Voltage control

The relationship between the currents in the inductors and the voltage in the PV modules can be obtained by means of the two remaining equations (3.13 and 3.15):

$$\begin{cases} \Delta \dot{V}_{pv2} = \frac{1}{2C}\left(\Delta I_{pv2} - \Delta I_{out} + (1 - D_1^o)\Delta I_{L1} - D_2^o\Delta I_{L2} - I_{L1}^o\Delta D_1 - I_{L2}^o\Delta D_2\right) = \frac{1}{C}\Delta I_{C2} \\ \Delta \dot{V}_{pv3} = \frac{1}{C}\left(\Delta I_{pv3} - \Delta I_{out} + (1 - D_2^o)\Delta I_{L2} - I_{L2}^o\Delta D_2\right) = \frac{1}{C}\Delta I_{C4} \end{cases}$$

The Laplace transform of the systems to be controlled are simply:

$$\begin{cases} \dfrac{I_{C2}}{V_{pv2}} = \dfrac{1}{Cs} \\[3ex] \dfrac{I_{C4}}{V_{pv3}} = \dfrac{1}{Cs} \end{cases} \tag{4.3}$$

And the rest of the currents can be feedforwarded as in figure 4-1 to improve the performance of the PI converters. However, and as can be noted, this would imply to use more sensors.

4.3 Results

The simulation results of the controlled circuit (fig 4-1) are depicted in figures 4-2 and 4-3. The irradiance level in the PV modules were:$Irr_1 = 1000\,W/m^2$ $Irr_1 = 600\,W/m^2$ $Irr_1 = 800\,W/m^2$. The voltages in PV modules 2 and 3 were commanded as shown in figure 4-2, where it can be seen a very fast response of the voltage controllers. Also, it can be noted that the changes in V_{pv3} and V_{pv2} commands are affecting both duties; in figure 4-3 the coupling between the converters can be appreciated very clearly in the currents. However, the PI regulators are doing their job, as the circuit variables are following the commanded voltage references. These voltage references can be obtained by implementing MPP tracking; the MPPT algorithm can be a standard incremental conductance, since the PI regulators are taking care of the decoupling of the converters.
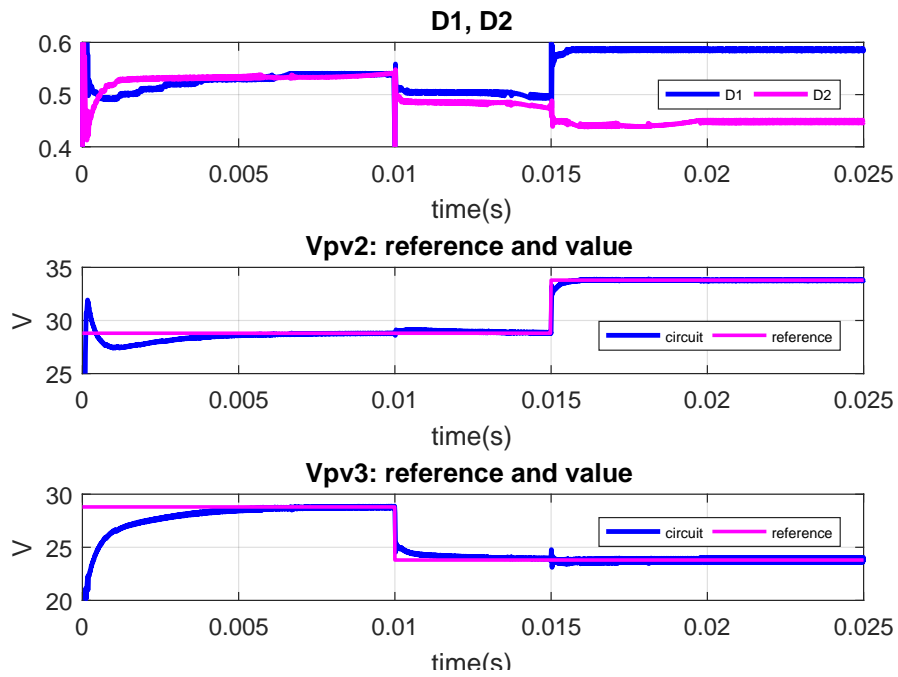
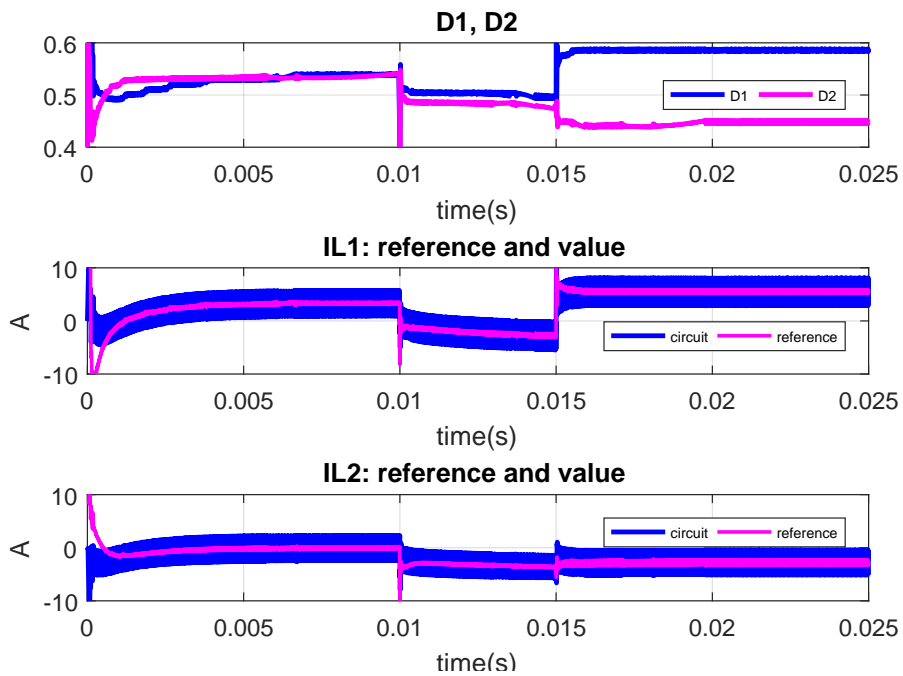Figure 4-2: Duty cycles and controlled voltages.

Figure 4-3: Duty cycles and controlled currents.

Chapter 5

Conclusions

It has been seen how for residential applications it makes more sense to implement the DPP architecture at submodular level, rather than at modular level, although the later has still some benefits. With little effort, the advantages -e.g., performance and efficiency- obtained over other topologies are very promising. However, the control of this kind of converters is not obvious at all. By modelling the converter, it has been demonstrated the high non linear nature of the topology, and the challenge of controlling such a coupled system. In spite of that, this situation could be overcome by implementing a simple cascaded control regulating the current in the inductors and the voltage in two of the three strings. However, it is needed another global MPPT in order to determine the third voltage, so if the submodular approach is chosen, a microinverter per module would be needed. With the modular approach, the central inverter would carry out that function.

It was desired to implement an experimental set-up in order to validate the concepts and conclusions accomplished, as well as an MPPT algorithm working along with the DPP operation. Then the DPP behaviour would be compared with the conventional topologies seen before, being able to extract further and more accurate conclusions regarding the actual improvement of the converter. However, this was not possible, since the linearization of the converter introduced so many problems, as it was demonstrated in the simulation results presented. Dealing with the unexpected high non-linearity of the DPP converter impeded the work to achieve the

scope desired in first place.

So, future research could be focused on the study of the conjunction of both modular and submodular DPP converters in the same installations for further improvements. Besides, it is still needed to determine the best MPPT algorithm for submodular DPPs with the control scheme here developed. Experimental implementation for validating the control approach followed in this thesis will be needed as well.

Bibliography

[1] S. Qin, C. B. Barth and R. C. N. Pilawa-Podgurski, "Enhancing Microinverter Energy Capture With Submodule Differential Power Processing,", in *IEEE Transactions on Power Electronics,*vol. 31, no. 5, pp. 3575-3585, May 2016. doi: 10.1109/TPEL.2015.2464235

[2] T. Esram and P. L. Chapman, "Comparison of Photovoltaic Array Maximum Power Point Tracking Techniques," in *IEEE Transactions on Energy Conversion,*vol. 22, no. 2, pp. 439-449, June 2007. doi: 10.1109/TEC.2006.874230

[3] H. J. Bergveld et al., "Module-Level DC/DC Conversion for Photovoltaic Systems: The Delta-Conversion Concept," in *IEEE Transactions on Power Electronics,*vol. 28, no. 4, pp. 2005-2013, April 2013. doi: 10.1109/TPEL.2012.2195331

[4] P. S. Shenoy and P. T. Krein, "Differential Power Processing for DC Systems," in *IEEE Transactions on Power Electronics,* vol. 28, no. 4, pp. 1795-1806, April 2013. doi: 10.1109/TPEL.2012.2214402.

[5] M. Alonso-Garcia, J. Ruiz, and F. Chenlo, "Experimental study of mismatch and shading effects in the iv characteristic of a photovoltaic module," *Solar Energy Materials and Solar Cells,* vol. 90, no. 3, pp.329–340, Feb. 2006.

[6] K. A. Kim, P. T. Krein, G. S. Seo and B. H. Cho, "Photovoltaic AC parameter characterization for dynamic partial shading and hot spot detection," *2013 Twenty-Eighth Annual IEEE Applied Power Electronics Conference and Exposition (APEC),* Long Beach, CA, USA, 2013, pp. 109-115. doi: 10.1109/APEC.2013.6520194

[7] K. Irisawa, T. Saito, I. Takano and Y. Sawada, "Maximum power point tracking control of photovoltaic generation system under non-uniform insolation by means of monitoring cells," *Conference Record of the Twenty-Eighth IEEE Photovoltaic Specialists Conference - 2000 (Cat. No.00CH37036),* Anchorage, AK, 2000, pp. 1707-1710. doi: 10.1109/PVSC.2000.916232

[8] K. Kobayashi, I. Takano and Y. Sawada, "A study on a two stage maximum power point tracking control of a photovoltaic system under partially shaded insolation conditions," *2003 IEEE Power Engineering Society General Meeting (IEEE Cat. No.03CH37491)* 2003, pp. 2617 Vol. 4. doi: 10.1109/PES.2003.1271058

[9] M. Bodur and M. Ermis, "Maximum power point tracking for low power photovoltaic solar panels," *Electrotechnical Conference, 1994. Proceedings., 7th Mediterranean,* Antalya, 1994, pp. 758-761 vol.2. doi: 10.1109/MELCON.1994.380992

[10] Yang Chen and K. M. Smedley, "A cost-effective single-stage inverter with maximum power point tracking," in *IEEE Transactions on Power Electronics,* vol. 19, no. 5, pp. 1289-1294, Sept. 2004. doi: 10.1109/TPEL.2004.833458

[11] R. Brown and M. Soldano, "One cycle control IC simplifies PFC designs," in *Twentieth Annual IEEE Applied Power Electronics Conference and Exposition, 2005. APEC 2005.,* Austin, TX, 2005, pp. 825-829 Vol. 2. doi: 10.1109/APEC.2005.1453075

[12] T. Shimizu, M. Hirakata, T. Kamezawa and H. Watanabe, "Generation control circuit for photovoltaic modules," in *IEEE Transactions on Power Electronics,* vol. 16, no. 3, pp. 293-300, May 2001. doi: 10.1109/63.923760

[13] T. Shimizu, O. Hashimoto and G. Kimura, "A novel high-performance utility-interactive photovoltaic inverter system," in *IEEE Transactions on Power Electronics,* vol. 18, no. 2, pp. 704-711, Mar 2003. doi: 10.1109/TPEL.2003.809375

[14] R. C. N. Pilawa-Podgurski and D. J. Perreault, "Submodule Integrated Distributed Maximum Power Point Tracking for Solar Photovoltaic Applications," in *IEEE Transactions on Power Electronics,* vol. 28, no. 6, pp. 2957-2967, June 2013. doi: 10.1109/TPEL.2012.2220861

[15] P. S. Shenoy, K. A. Kim, B. B. Johnson and P. T. Krein, "Differential Power Processing for Increased Energy Production and Reliability of Photovoltaic Systems," in *IEEE Transactions on Power Electronics,* vol. 28, no. 6, pp. 2968-2979, June 2013. doi: 10.1109/TPEL.2012.2211082

[16] C. Olalla, C. Deline and D. Maksimović, "Modeling and simulation of conventionally wired photovoltaic systems based on differential power processing SubMIC-enhanced PV modules," *2014 IEEE 15th Workshop on Control and Modeling for Power Electronics (COMPEL),* Santander, 2014, pp. 1-9. doi: 10.1109/COMPEL.2014.6877127

[17] MathWorks online help, *https://es.mathworks.com/help/physmod/sps/powersys/ref/pvarray.html*

[18] S. Qin, S. T. Cady, A. D. Domínguez-García and R. C. N. Pilawa-Podgurski, "A distributed approach to MPPT for PV sub-module differential power processing," *2013 IEEE Energy Conversion Congress and Exposition,* Denver, CO, 2013, pp. 2778-2785. doi: 10.1109/ECCE.2013.6647061